References

1. Van Harlingen, D. J. (1995) *Review of Modern Physics* **67**, 515.
2. Barone, A. (1994) *Il Nuovo Cimento* **16 D**, 1635.
3. Yip, S. (1990) *Physical Review* **B 41**, 2612; (1990) *Journal of Low Temperature Physics* **31**, 129.
4. Maki, K. and Won, H. (1994) *Physical Review Letters* **72**, 1738; Won, H. and Maki, K. (1994) *Physical Review* **B 49**, 15305.
5. Tanamoto, T., Kohno, H. and Fukuyama, H. (1992) *Journal of Physics of Japanese Society* **61**, 1886.
6. Aronov, A.G., Hikami, S. and Larkin, A.I. (1989) *Physical Review Letters* **62**, 965; (1989) **62**, 2336(E); Bieri, J.B. and Maki, K. (1990) *Physical Review* **B 42**, 4854; Bieri, J. B., Maki, K. and Tompson, R.S. (1991) *Physical Review* **B 44**, 4709.
7. Latyshev, Yu.I., Laborde, O. and Monceau, P. (1995) *Europhysics Letters* **29**, 495.
8. Balestrino, G., Milani, E. and Varlamov, A.A. (1995) *Pis'ma Zh. Eksp. Teor. Fiz.* **61**, 814.
9. Kuboki, K. and Fukuyama, H.J. (1989) *Physical Japanese Society* **58**, 376.
10. Randeria, M. and Varlamov, A.A. (1994) *Physical Review* **B 50**, 10401.
11. Dorin, V.V., Klemm, R.A., Varlamov, A.A., Buzdin, A.I. and Livanov, D.V. (1993) *Physical Review* **B 48**, 12951.
12. Müller, K.A. (1995) *Nature* 377, 133.

MEASUREMENTS OF THE FREQUENCY DEPENDENT MICROWAVE FLUCTUATION CONDUCTIVITY OF CUPRATE THIN FILM SUPERCONDUCTORS

JAMES C. BOOTH, DONG-HO WU, and STEVEN M. ANLAGE
Physics Department
Center for Superconductivity Research
University of Maryland
College Park, MD 20742-4111 USA
(anlage@squid.umd.edu, http://www.csr.umd.edu)

1. Overview and Surface Impedance Measurements of Superconductors

We describe our measurements of the fluctuation lifetime in high-T_c superconducting thin films above T_c. The paper is laid out as follows. Section 1 discusses our our motivation and broadband experimental technique, while sections 2 and 3 present the experimental method in detail. Section 4 is a brief discussion of the electromagnetic fields used in our experiment. Section 5 presents and discusses the data on fluctuation conductivity, and summarizes our observations regarding the nature of fluctuations above T_c in the cuprate superconductors. Finally, section 6 serves as a conclusion.

Surface impedance measurements at microwave frequencies have historically provided a wealth of essential information about the fundamental properties of the superconducting state.[1,2] Microwave experiments typically have very high sensitivity, allowing for detailed measurements of the very low losses characteristic of superconductors. In addition, measurements at finite frequencies allow for the determination of the electrodynamic response of both the superconducting condensate as well as the quasiparticle excitations that exist at finite temperatures. Microwave measurements have the advantage that the frequency is still well below the maximum gap frequency, and contributions from both the condensate and the quasiparticles are large enough to be measurable.

In recent years, microwave surface impedance measurements have played a vital role in the ongoing effort to understand the mechanism of superconductivity in the newly discovered high transition temperature (high T_c) superconductors.[3,4] In particular, microwave penetration depth measurements on single crystals have provided compelling evidence in the effort to determine the symmetry of the order parameter in the high T_c materials.[5,6] Microwave measurements also provide a very stringent test of sample quality, and are therefore well suited to help separate intrinsic and extrinsic effects in these exotic and complicated materials, and also aid considerably in efforts to improve the quality of these materials.[7]

In addition to fundamental aspects such as the pairing state symmetry of the high T_c superconductors, microwave measurements can also be used to help develop a general phenomenological picture of superconductivity in these materials, in the absence of a fundamental theory. Microwave techniques have also been used extensively in studying the dynamic properties of magnetic vortices in the mixed state of the high T_c superconductors, and can be used to determine the relevant physical parameters of these materials, such as the lower critical field $H_{c1}(T)$.[8]

The main focus of this paper is on microwave experiments that explore the

M. Ausloos and A.A. Varlamov (eds.),
Fluctuation Phenomena in High Temperature Superconductors, 151–178.

frequency dependence of the electrodynamic properties of high T_c superconductors. In what follows, the difference in approach between resonant and broadband microwave measurements is discussed, with the emphasis being placed on measurements of the non-resonant variety. This is followed by some motivation as to what can be learned from broadband measurements applied to the high T_c superconductors.

1.1. BROADBAND SURFACE IMPEDANCE MEASUREMENTS

Non-resonant experiments at microwave frequencies typically measure the transmission or reflection of a microwave signal incident on the sample. Since they do not make use of a resonant mode, there is much more freedom in choosing an operating frequency in these experiments than in their resonant counterparts. Some of the most important early microwave measurements on superconductors were the transmission measurements of Glover and Tinkham[2]. Broadband measurements are usually much less sensitive than high-Q resonant measurements, because the measured quantity is typically a voltage, not a frequency. In addition, in order to accurately measure both the real and imaginary parts of the response, one must use phase-sensitive measurement techniques, which become increasingly more difficult as the measurement frequency increases and the signal wavelength becomes much smaller than the measurement apparatus.

The measurement system described in this paper is a broadband type, but is different from waveguide transmission measurements in a number of significant ways. Our technique, referred to as the Corbino reflection technique,[9] measures the complex reflection coefficient (from 45 MHz - 50 GHz) of a thin film which forms an electrical short circuit across a coaxial transmission line. The Corbino reflection technique is a swept-frequency method, which allows for the direct measurement of the full complex resistivity (or conductivity) of thin film samples as a function of frequency over three decades in the rf/microwave/mm wave range. The measurement utilizes the TEM mode in a coaxial geometry in order to maximize the frequency range accessible to the measurement. The coaxial transmission lines used here support exclusively the TEM mode up to approximately 70 GHz, and can be used at frequencies all the way down to dc due to the absence of a lower cutoff frequency for the TEM mode. The use of the TEM mode also results in a relatively simple field distribution within the thin film sample. Also, for the geometries used here, the measured reflection coefficient is rather simply related to the complex resistivity of the sample, which is a fundamentally interesting quantity.

1.2 FREQUENCY DEPENDENT MICROWAVE MEASUREMENTS

There are many fundamentally and practically interesting phenomena that can be studied using frequency dependent measurements in the microwave range. Access to the frequency dependence provides direct information about the time dependence of the system under study. If there are physical processes that take place on time scales of the order of 1/f seconds (where $4.5 \times 10^7 \leq f \leq 5 \times 10^{10}$), then one can expect the frequency response of the system to change as the frequency is swept through the current measurement range. Due to the fact that most microwave measurements are resonant in nature, phenomena at microwave frequencies have been primarily viewed from a fixed frequency point of view. As will be shown throughout this work, access to the frequency dependence can give a different and often valuable new perspective on physical phenomena.

2. The Corbino Reflection Measurement Technique

2.1 THE CORBINO DISK GEOMETRY

Here we describe the experimental technique which allows the surface impedance of superconducting thin films to be measured at arbitrary frequencies in the rf and microwave range (from 45 MHz - 50 GHz). Measurements at lower frequencies have been accomplished using other methods.[10-12] The measurement technique, shown schematically in Fig. 2.1, employs a vector network analyzer to measure the complex reflection coefficient (S_{11}) of a thin film which forms an electrical short circuit across the end of a coaxial cable. Once the complex reflection coefficient is measured, standard transmission line theory is used to extract the complex surface impedance of the film from S_{11}.[13] The measurement takes advantage of a special geometry in which the sample forms a thin disc between the inner and outer conductors of the coaxial cable. The use of such a measurement geometry -- referred to as a Corbino disk[14] geometry -- means that currents in the film flow in the radial direction, producing magnetic fields only in the azimuthal direction, everywhere parallel to the surface of the film. The effects of the edges of the film are therefore effectively eliminated in the Corbino geometry (compare with a rectangular or microbridge geometry, where self fields due to the current can be perpendicular to the film surface, particularly at the edges). This geometry is particularly beneficial when studying the motion of magnetic vortices in the mixed state of superconductors, since the sample edge contribution to the creation and/or pinning[15] of vortices has been eliminated. An additional advantage of the technique is that it allows for the surface impedance to be determined over a wide range of experimental parameters, including temperature, magnetic field, frequency, rf power, and dc bias current.

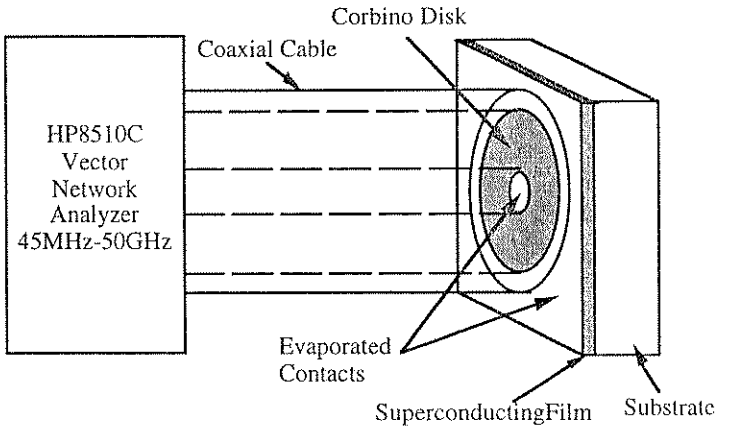

Fig. 2.1. Schematic diagram of Corbino measurement configuration

The Corbino reflection measurement technique developed out of the historical use of the Corbino geometry for dc transport measurements.[14] Bluzer and collaborators[16] used the Corbino geometry to measure time-domain picosecond quasiparticle dynamics in zero field in low- and high- T_c superconducting films. Their basic technique has been adapted to the frequency domain, and to the study of vortex dynamics and fluctuation conductivity in high T_c superconductors.

This section describes in detail the application of the Corbino reflection

technique to measurements of the surface impedance of superconducting thin films. Section 2.2 gives an overview of the experimental technique used in this work, and section 2.3 will give a description of the crucial interface region between the coaxial transmission line and the thin film under study. Section 2.4 will then discuss the details of the preparation of superconducting thin film samples for the measurements presented here, and section 2.5 will briefly describe the dc resistivity measurements used to complement the microwave experiments.

2.2 EXPERIMENTAL OVERVIEW

Two different experimental set-ups are used to measure the reflection coefficient, depending on whether or not an external dc magnetic field is required. For both experimental configurations, the thin film under study is used to terminate a coaxial transmission line, and the complex reflection coefficient S_{11} is measured over the continuous frequency range 45 MHz - 50 GHz using a Hewlett-Packard HP8510C vector network analyzer. The microwave source is a Hewlett-Packard HP83651A synthesized sweeper which operates over the frequency range 45 MHz - 50 GHz with 1 Hz resolution. The network analyzer is operated in step sweep mode to ensure phase coherence at each frequency point. Related experimental techniques use reflection coefficient measurements to obtain the complex dielectric constant of liquids[17,18] and solids[19,20] at room temperature. In our case, the dependence of the reflection coefficient on temperature, magnetic field, and frequency is of primary interest.

In addition to measurements at rf and microwave frequencies, this technique also allows for 2-point dc measurements to be performed. A dc bias current is applied to the coaxial cable, and the resulting voltage drop between the inner and outer conductors of the coaxial cable is measured at the location of the network analyzer (an rf choke internal to the HP8510C test set protects the high frequency detectors from the dc current). This ability to make dc measurements simultaneously with the microwave measurements is important because it allows direct comparison of the high frequency response with the more conventional dc behavior.

Fig. 2.2 shows schematically the experimental set-up used for measurements in zero external magnetic field. The sample is mounted on the cold finger of a Janis model ST-100 continuous-flow cryostat, and is connected to the network analyzer by means of a 0.086 inch outer diameter copper coaxial transmission line, which supports only the TEM mode up to approximately 70 GHz. The dielectric material for the coaxial transmission line is air-articulated PTFE (Teflon), which is used because it has the best available combination of thermal and electrical properties. A number of other coaxial cables with differing dielectric materials were tried, including solid PTFE and Isocore brand[21] PTFE. It was found experimentally that the solid PTFE was considerably more noisy, due to the expansion and contraction of the solid dielectric. The Isocore PTFE had by far the best thermal properties, but the phase velocity changed unpredictably with time at low temperatures. In this experimental configuration, the copper coaxial cable was a severe heat load for the system, and a stainless steel transmission line would have been preferable, but a stainless steel coaxial cable with the required air-articulated PTFE dielectric was not available. In order to minimize attenuation effects at higher frequencies, the transmission line is kept as short as possible, ~ 22 cm for the zero-field measurements.

To control the temperature, a silicon diode thermometer was mounted on the cold finger, and a Lakeshore model DRC-93CA temperature controller was used to stabilize the temperature at the desired value. The temperature of the sample was monitored by an additional temperature sensor located on the cylindrical copper sample housing, because large temperature gradients can be present in this experimental configuration.

Before the sample is loaded into the cryostat, room temperature calibrations are performed directly at the position of the sample at the termination of the transmission line. Then the sample is connected first to the transmission line, and then to the cold finger of the cryostat. The main advantage of this set-up, other than the short transmission line, is the fact that after the transmission line is calibrated, the sample can be connected without disconnecting the transmission line from the test set. This provides the maximum accuracy, and a high quality calibration is crucial for an accurate measurement over such a wide frequency range. After the sample is attached to the cold finger, the cryostat is pumped down to a pressure of ~20 μm Hg before the helium transfer is begun. During the entire measurement, a continuous flow of liquid helium is maintained through the cryostat in order to achieve the necessary cooling power.

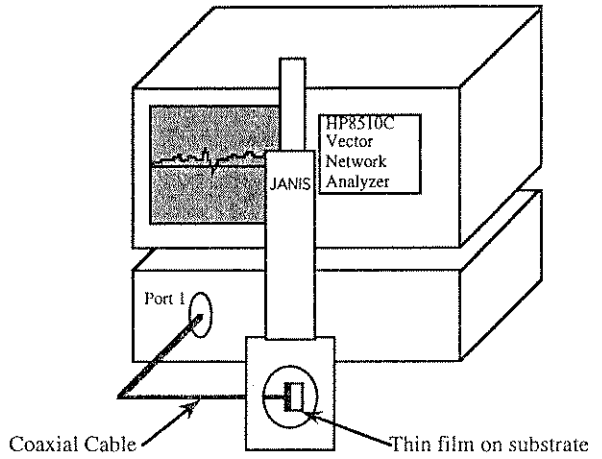

Fig. 2.2. Schematic diagram of experimental set-up for measurements in zero applied magnetic field.

Measurements are performed in this configuration by slowly ramping the temperature set point up from its initial value. After the temperature is stabilized at each set point, the frequency dependent reflection coefficient is measured. From the full frequency dependence (usually consisting of 201 frequency points), several values of the reflection coefficient at preselected frequencies are written to a temperature dependent file, and the entire frequency trace is saved at periodic intervals. The data set from a given temperature ramp therefore consists of a file with the temperature-dependence of the reflection coefficient at several fixed frequencies, and a number of files containing the entire frequency dependence at different temperatures.

2.3 COAXIAL CABLE/THIN FILM INTERFACE

A detailed diagram of the coaxial cable/film interface is shown in Fig. 2.3. Gold contacts a few thousand angstroms thick are evaporated through a washer-shaped shadow mask to form inner and outer electrical contacts on the film. The portion of the film exposed between the contacts forms the Corbino disc proper, the inner and outer diameters of which are approximately 0.020 and 0.066 inch, respectively. Electrical contact is made to the inner and outer conductors of the coaxial cable through a modified microwave connector.[22] Direct contact is made between the outer conductor of the connector and the outer contact of the film, while contact is made between the inner

contact of the film and the inner conductor of the cable by means of a small tapered pin inserted into the connector center conductor. The pin is tapered from a diameter of 0.020" down to 0.010", so that there is a restoring force in the direction of the film (the center conductor of the microwave connector is designed to spread open slightly in order to capture the center conductor of the mating connector), to ensure that contact is maintained as the temperature is lowered. The size of this center conductor pin is crucial; if the diameter at the large end is much less that 0.020" the pin slides into the connector center conductor, and there is no restoring force. If the large end diameter is much greater than 0.020" the pin becomes a large perturbation within the connector, and can cause large resonant effects which make accurate frequency dependent measurements impossible. Contact is maintained as the temperature is changed by means of a copper pedestal and spring assembly which apply pressure to the backside of the substrate. Such a contact can reliably hold from room temperature to 4.2 K, with changes in the contact resistance of at most 15 mΩ over the entire temperature range.

In order to align the contacted film with the microwave connector properly, a special alignment jig is used to position the sample on the copper pedestal. Once the film is correctly positioned, the entire film/pedestal assembly[16] is loaded into a cylindrical copper housing, which also accepts the microwave connector, and ensures that the contacts on the film align with the connector as shown in Fig. 2.3.

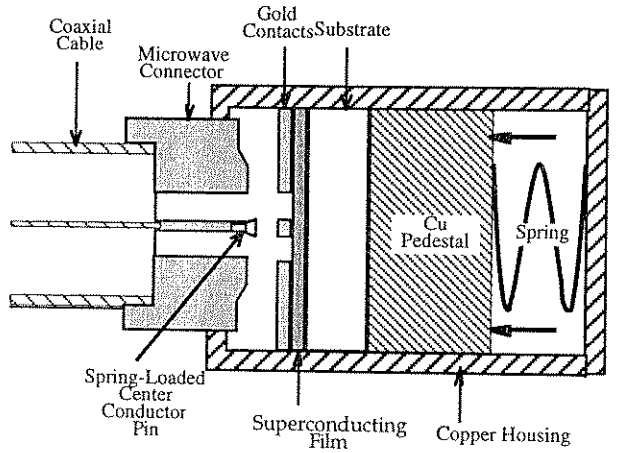

Fig. 2.3. Detailed view of thin film/connector interface, just prior to contact. Pressure is exerted on the aluminum pedestal by a spring in order to maintain contact between the film and connector throughout the temperature range.

In the Corbino disk geometry the rf currents flow in the radial direction, and the rf current density in the film is proportional to 1/r, where r is the distance from the center of the Corbino disk. The rf current density also depends on the film thickness and the rf power supplied by the source. If the sample is much thinner than the appropriate skin depth, the current density will be uniform in the film thickness. The (instantaneous) power transferred along the transmission line is given by the Poynting vector $\mathbf{P} = (\mathbf{E} \times \mathbf{H}^*)$ integrated over the cross section of the transmission line, which gives simply $P=I \cdot V$. The ratio of the voltage to the current is simply the characteristic impedance of the transmission line, $P=I^2 Z_0$. The current density J is found by demanding that J(r) integrated over the volume of the Corbino disk be equal to the

applied current I, which gives $J(r) = I/2\pi t_0 r$, where t_0 is the film thickness. The peak current density in the sample as a function of microwave power is therefore given by

$$J(r) = \frac{1}{2\pi t_0 r}\sqrt{\frac{P}{Z_0}} \qquad (2.1)$$

As an example, for a 1000 Å thick film and an applied rf power (at the sample) of zero dBm (=1 mW), and assuming the current density is uniform throughout the film thickness, the peak current density in the film is approximately 3×10^3 amps/cm^2.

2.4 SAMPLE PREPARATION

The superconducting thin films studied in this work are primarily several thousand angstroms of $YBa_2Cu_3O_{7-\delta}$ (YBCO) deposited on $LaAlO_3$ substrates (1/4" x 1/4" square, typically) by pulsed laser deposition.[23] Thin film samples were obtained from A. Findikoglu, C. Kwon, and M. Rajeswari within the Center for Superconductivity Research, and also from Alberto Pique at Neocera, Inc.

In order to make concentric gold or silver contact pads as shown in Figs. 2.1 and 2.3, two different approaches were used: *in-situ* and *ex-situ* contact deposition. In the *ex-situ* technique a washer shaped shadow mask is used during evaporation of the contacts. The shadow mask is made from a magnetic material called COVAR which is an alloy of cobalt, nickel and iron, and is held in place by means of small magnets embedded in a specially designed substrate holder. The gold or silver is evaporated thermally or by electron beam evaporation, forming the inner and outer contact pads, and the masked part of the film becomes the Corbino disk. If the contact resistance between the gold or silver and YBCO is unsatisfactorily high (≥ 25 mΩ), as determined by a 3-point resistivity measurement when the film is superconducting (see section 2.5 below), the film is annealed in O_2 at 400-450 C for 1-8 hours. This normally results in a contact resistance of less than 15 mΩ (which gives a contact resistivity of approximately 3×10^{-5} Ωcm^2, assuming that the contact resistance is dominated by the smaller center contact). However, it is very important to ensure that no impurities are introduced during the contacting or annealing steps, since the subsequent annealing can destroy superconductivity in the film if some contamination has occurred.

The *ex-situ* technique described above was used for most of the samples studied in this work. However, an *in-situ* technique was also investigated. For the *in-situ* technique, a gold contact layer is deposited immediately following the film deposition before the film is exposed to the atmosphere. After deposition a Corbino disk pattern is transferred to the gold/YBCO bilayer by standard photolithography techniques, and the gold is removed from the Corbino disk region using a gold etch (1g K/ 4g KI in 80 ml deionized water). While the contact resistances were generally acceptable and no additional annealing was required, the samples subject to the *in-situ* process appeared to have been slightly damaged by the etching step. In order to be useful for the measurements described here, further optimization of the *in-situ* technique is required.

2.5 DC RESISTIVITY MEASUREMENTS

Measurements of the dc resistivity vs. temperature are made independently of the microwave measurements discussed above and serve several purposes. The temperature dependent resistivity measurements can be performed in about an hour, and are used to screen films so that only the best quality samples are used in the microwave measurements. Also, the dc measurements provide a sensitive measure of the contact resistance, which cannot be determined from the two-point resistance values obtained

during the microwave measurements, and is difficult to determine directly from the microwave data. The dc measurements also serve as a check on the microwave surface impedance values, since in the thin film limit the real part of the effective impedance is just the real part of the resistivity, which is simply the dc resistivity for a thin normal metal. In addition, the dc resistivity measurements can be easily performed up to room temperature (which is difficult in the microwave setup), and can be instrumental in determining the temperature dependence of normal state properties for fluctuation conductivity analysis, for example.

3. Measurement Calibration and Error Correction

In this section a brief outline is given of the analysis procedures developed to correctly interpret the measured frequency dependent data on superconducting thin films. One must first perform standard microwave calibration procedures at room temperature that are necessary for the accurate frequency measurement of the complex reflection coefficient $S_{11}(\omega)$ over the broad frequency range from 45 MHz - 50 GHz. To apply this calibration to low-temperature measurements, one must then examine the errors associated with such a calibration procedure, and also consider the effect of errors that affect the frequency dependent measurements that are not addressed by standard calibration procedures, such as changes in the temperature of the transmission line, and transmission of the incident signal through the thin film under study and into the substrate. Once an accurate measurement of the complex reflection coefficient is obtained, the frequency-dependent surface impedance is easily extracted. After taking into account the effect of the finite thickness of the measured thin film, the complex resistivity $\rho(\omega) = \rho_1(\omega) + i\rho_2(\omega)$ is obtained. The full error correction procedure we have developed for accurate frequency dependent measurements of the complex resistivity of thin films at cryogenic temperatures is summarized in reference [24].

4. Electromagnetic Field Distribution in the Corbino Geometry

Broadband measurements in the microwave regime can be utilized to gain important information about the frequency dependence of the electrodynamic response of a wide range of materials. One approach to broadband measurements is to use the TEM mode in a coaxial waveguide in order to avoid the restriction of operating above a fixed cutoff frequency. There exist many examples of measurements that utilize an open-ended coaxial probe in order to measure dielectric constants of solids,[19] liquids,[17,25] and even living tissue.[18,26,27]

The particular geometry that is used in this work is shown in Fig. 4.1, and corresponds to an abrupt coaxial to circular waveguide transition (the cylindrical copper housing shown in Fig. 2.3 corresponds to the circular waveguide section). Calculations of the frequency response of such a discontinuity have been accomplished using a number of different theoretical techniques.[20,28,29] We have developed a calculation based on a mode-matching technique that is used to mathematically model the frequency response in this geometry, in order to better understand the measured data obtained on superconductors.[24] In particular, it is desirable to be able to calculate the effect of radiation propagating through a metallic or superconducting thin film sample into the substrate in the Corbino geometry, in order to understand the frequency response of the substrate effect. In addition, such a calculation could be used to model the response of more complicated samples, such as superconductor/insulator structures and multilayers.

The objective of this calculation is to obtain an expression for the frequency-dependent reflection coefficient $S_{11}(\omega)$ at the location of the transition (z=0 in Fig. 4.1)

for the general case of an arbitrary combination of metallic (or superconducting) and/or dielectric layers in the circular waveguide region (region 2). To accomplish this, first the normal modes for the two waveguide regions are calculated from Maxwell's equations. The general mode-matching technique is then used to calculate the reflection coefficient of the TEM mode at the discontinuity, and the coupling coefficients between the coaxial waveguide modes and the circular waveguide modes are calculated. Next, the frequency-dependent reflection coefficient is calculated for a number of different uniform dielectric materials filling the circular guide (including air, Teflon, and sapphire), and compared with actual measurements of these materials. Finally, the substrate effect for thin metallic layers is modeled, and the frequency dependence of the substrate impedance is calculated and compared to that derived from actual measurements. Further details of these calculations are presented in reference [24].

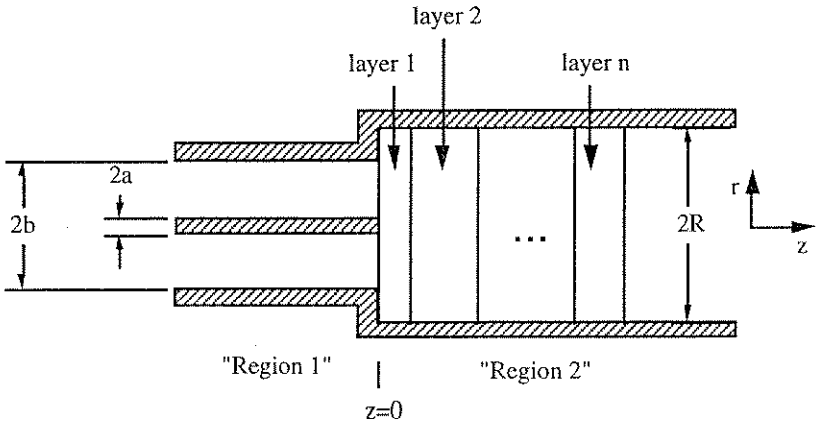

Fig. 4.1. Schematic diagram of coaxial/circular waveguide interface.

5. Fluctuation Effects in the Conductivity of YBCO Thin Films

5.1 INTRODUCTION -- FLUCTUATIONS IN SUPERCONDUCTORS

Fluctuation effects in the vicinity of phase transitions have drawn much interest in recent years. In the high temperature superconductors it is believed that fluctuation effects are larger, and the region of temperature over which they are important is much wider than in their low temperature counterparts, allowing for fluctuations to be studied in far greater detail in these superconducting systems.[30] The high T_c superconductors may also provide the opportunity to measure critical behavior near the superconducting phase transition,[31] which is precluded in the low T_c systems because the critical regime is unobservably narrow.

The effects of thermal fluctuations near a critical point can be observed in a number of different experimental quantities, such as the specific heat, susceptibility, dc conductivity, etc. In this section the effects of fluctuations on the microwave conductivity of high T_c superconductors (primarily above T_c) are investigated in detail.

This section describes a systematic study of dynamical fluctuation effects in the temperature and frequency dependent conductivity of YBCO thin films measured over

three decades of frequency in the microwave range (45 MHz - 45 GHz). Previous observations of the ac fluctuation conductivity have been reported in the temperature dependence of the conductivity of thin lead films at (discrete) microwave frequencies by Lehoczky and Briscoe[32], while Tanner measured the frequency dependence of the fluctuation conductivity at far-infrared frequencies, also using thin lead films.[33] Both experimental studies found quantitative agreement with the 2D Gaussian fluctuation theory, based on time dependent Ginzburg-Landau theory. Previous work on fluctuation conductivity in the cuprates has focused mainly on dc resistivity vs. temperature measurements in YBCO crystals,[34-36] where the measured data was best fit by the 2D Gaussian fluctuation theory well above T_c and 3D Gaussian theory closer to T_c. Recently there have been reported measurements of the zero-field fluctuation conductivity at finite frequency in YBCO, observed in the temperature dependence of the conductivity above T_c at 9.6 GHz on single crystals.[37] These measurements also showed 2D Gaussian fluctuations for $T > T_c$, consistent with the dc measurements.

Critical fluctuation effects can be observed when fluctuations become sufficiently large so that the Gaussian approximation treatment of the Ginzburg-Landau free energy is no longer valid. The critical region is identified experimentally by measuring quantities such as the fluctuation lifetime t^{fl} and correlation length ξ, which diverge differently than predicted by the Gaussian theory as $T \rightarrow T_c$ within the critical region. Evidence of critical behavior in the cuprate superconductors has been reported in the temperature dependence of the microwave penetration depth of YBCO single crystals as T_c is approached from below.[37,38] Such measurements reveal a surprisingly wide critical region below T_c (~ 5-10 K), which exhibits 3D XY critical behavior. Heat capacity data also show 3D XY behavior [-0.03 < (2-Dv) <0] for $T = T_c \pm 10$ K.[39] Above T_c there has been no definitive observation of critical effects in the high T_c materials in zero magnetic field. Efforts to observe critical behavior in temperature-dependent conductivity measurements are hampered by the inability to measure closely enough to T_c and are also often clouded by the question of sample homogeneity. It is therefore very important to explore different experimental degrees of freedom in order to determine if a critical region exists above T_c in the high T_c materials, and if so, what are the critical exponents and scaling functions that describe the approach to the phase transition.

The ability of the Corbino reflection technique to extract the frequency dependence of the conductivity in addition to the temperature dependence at temperatures through T_c provides additional essential information on the nature of the phase transition at T_c. By measuring the frequency dependence of the magnitude and phase of the fluctuation contribution to the conductivity, we can extract a measure of the thermodynamic critical temperature and the dynamical critical exponent z (both of which are difficult to determine using solely the temperature dependence). This fact has been utilized in lower frequency measurements to locate a phase transition from a vortex liquid to a vortex solid in finite fields in YBCO films[40-42] and in Mo_3Si films[43], where the characteristic time scales are longer. Our access to the frequency dependence also allows us to directly observe the effect of the finite fluctuation lifetime on the conductivity above T_c, and also to determine how that lifetime diverges as $T \rightarrow T_c$ in an effort to identify critical phenomena.

In what follows, we will first describe in section 5.2 the current theoretical understanding of fluctuation effects in superconductors. This will be followed in section 5.3 with a detailed analysis of the temperature dependence of the dc resistivity, with the goal of obtaining a measure of the normal state or mean-field contribution to the experimentally measured conductivity. In section 5.4 the frequency dependence of the complex conductivity in the immediate region of the superconducting phase transition will be analyzed in terms of the fluctuation theories outlined above, and in section 5.5 the temperature dependence of the fluctuation contribution to the conductivity will be explored. Finally in section 5.6 the dependence of the fluctuation effects on sample quality will be addressed by analyzing the fluctuation conductivity of samples of varying quality.

5.2 MODELS OF FLUCTUATIONS IN SUPERCONDUCTORS

5.2.1 *Mean-field Theory: Ginzburg-Landau Theory*

This section gives a brief summary of the application of Ginzburg-Landau (GL) theory to calculate the effect of fluctuations of the order parameter on the conductivity of a superconductor. This section is not meant to be a complete description of Ginzburg-Landau theory; more complete treatments are available from a number of sources.[44-47] Our goal in this section is simply to identify the relevant length and time scales as they appear in Ginzburg-Landau theory. In addition, the resulting expressions for the fluctuation conductivity in three dimensions derived from time-dependent Ginzburg-Landau (TDGL) theory will be presented, followed by the corresponding expressions valid for two dimensions.

The relevant length scale for the problem is the Ginzburg-Landau correlation length ξ_{GL}, derived from time-independent Ginzburg-Landau theory and which is defined in the Gaussian limit by

$$\xi(T) = \left(\frac{\hbar^2}{2m^*|\alpha|}\right)^{1/2} = \frac{\xi_0}{|\varepsilon|^{1/2}} \qquad (5.1)$$

where $\varepsilon = \ln(T/T_c) \approx (T-T_c)/T_c$. The meaning of ξ physically can be seen by considering the spatial correlation function of the order parameter $g(\mathbf{r},\mathbf{r'}) = \langle \psi^*(\mathbf{r})\psi(\mathbf{r'})\rangle$. Writing the relative coordinate $\mathbf{R} = \mathbf{r} - \mathbf{r'}$, valid for a homogeneous system, gives the result

$$g(R) = \frac{m^* k_B T}{2\pi\hbar} \frac{\exp\left(-R/\xi(T)\right)}{R} \qquad (5.2)$$

This gives spatial correlations of the order parameter which fall off exponentially over a length scale defined by $\xi(T)$. The quantity $\xi(T)$ therefore gives approximately the spatial extent of the fluctuations.

In order to calculate the effect of fluctuations of the order parameter on the conductivity, it is necessary to include a time dependence in the Ginzburg-Landau free energy, since the excess conductivity due to fluctuations will be directly proportional to the lifetime of the fluctuations. The simplest time dependent generalization of the time-independent Ginzburg-Landau theory introduces a temperature-dependent relaxation time, given by

$$\tau_{GL} = \frac{\hbar\gamma}{\alpha} = \frac{\tau_0}{|\varepsilon|} \qquad (5.3)$$

The time dependent Ginzburg-Landau formalism can be used to calculate the contribution to the conductivity of superconducting fluctuations. Such a calculation has been carried out by Schmidt,[48] and later by Dorsey[49]. The results for the fluctuation conductivity ($\sigma = \sigma_1 - i\,\sigma_2$) depend upon the dimensionality of the system, and are given in three dimensions by

$$\sigma_1^{3D} = \sigma_{DC}^{3D} \cdot F_1^{\pm}(\omega\tau)$$
$$\sigma_2^{3D} = \sigma_{DC}^{3D} \cdot F_2^{\pm}(\omega\tau) \qquad (5.4)$$

Here $F_1^{\pm}(\omega\tau)$ and $F_2^{\pm}(\omega\tau)$ describe the frequency dependence above (+) and below(-) T_c, and σ_{DC} is the dc fluctuation conductivity given by

$$\sigma_{DC}^{3D} = \frac{e^2}{32\hbar\xi_0\,\varepsilon^{1/2}} \qquad (5.5)$$

where once again $\varepsilon=\ln(T/T_c)$. The expression for the dc fluctuation conductivity was first worked out by Aslamazov and Larkin.[50] In three dimensions, the frequency dependent functions F^+ are given for $T > T_c$ by

$$F_1^+(\omega\tau) = \frac{8}{3(\omega\tau)^2}\left[1 - \left(1+(\omega\tau)^2\right)^{3/4}\cdot\cos\left(\frac{3}{2}\cdot\tan^{-1}(\omega\tau)\right)\right]$$
$$F_2^+(\omega\tau) = \frac{8}{3(\omega\tau)^2}\left[-\frac{3}{2}\omega\tau + \left(1+(\omega\tau)^2\right)^{3/4}\cdot\sin\left(\frac{3}{2}\cdot\tan^{-1}(\omega\tau)\right)\right] \qquad (5.6)$$

The functions F^- for $T < T_c$ are given below for reference, also in three dimensions

$$F_1^-(\omega\tau) = \frac{8}{3(1+\omega\tau)^2}\left[\sqrt{2} - \left(1+(\omega\tau)^2\right)^{-1/4}\cdot\left\{\left(1-(\omega\tau)^2\right)\cdot X + 2\omega\tau Y\right\}\right]$$
$$F_2^-(\omega\tau) = \frac{8}{3(1+\omega\tau)^2}\left[-\sqrt{2} + 2\left(1+(\omega\tau)^2\right)^{-1/4}\cdot\left\{X - \frac{\left(1-(\omega\tau)^2\right)}{2\omega\tau}Y\right\}\right] \qquad (5.7)$$

where $X=\cos[(1/2)\cdot\tan^{-1}(\omega\tau)]$, and $Y=\sin[(1/2)\cdot\tan^{-1}(\omega\tau)]$. The fluctuation relaxation time τ is given by

$$\tau = \frac{\pi\hbar}{16k_B T_c\,\varepsilon} \qquad (5.8)$$

In two dimensions the results for the fluctuation conductivity are given by the following

$$\sigma_1^{2D} = \sigma_{DC}^{2D} \cdot G_1^{\pm}(\omega\tau)$$
$$\sigma_2^{2D} = \sigma_{DC}^{2D} \cdot G_2^{\pm}(\omega\tau) \qquad (5.9)$$

where once again the functions $G^{\pm}(\omega\tau)$ describe the frequency dependence, and the two-dimensional dc fluctuation conductivity is given by

$$\sigma_{DC}^{2D} = \frac{e^2}{16\hbar d\,\varepsilon} \qquad (5.10)$$

Here d is the film thickness. The frequency dependent functions G^+ for $T > T_c$ in two dimensions are

$$G_1^+(\omega\tau) = \frac{1}{\omega\tau}\left[\pi - 2\tan^{-1}\left(\frac{1}{\omega\tau}\right) - \frac{1}{\omega\tau}\cdot\ln\left(1+(\omega\tau)^2\right)\right]$$
$$G_2^+(\omega\tau) = \frac{1}{\omega\tau}\left[-2 + \frac{\pi}{\omega\tau} - \frac{2}{\omega\tau}\tan^{-1}\left(\frac{1}{\omega\tau}\right) + \ln\left(1+(\omega\tau)^2\right)\right] \qquad (5.11)$$

while the corresponding expressions for $T < T_c$ are

$$G_1^-(\omega\tau) = \frac{\omega\tau}{(1-\omega\tau)}\left[\pi - 2\tan^{-1}\left(\frac{1}{\omega\tau}\right) - \frac{1}{\omega\tau}\cdot\ln\left(\frac{1+(\omega\tau)^2}{4}\right)\right]$$
$$G_2^-(\omega\tau) = \frac{1}{(1-\omega\tau)}\left[\pi - 2\tan^{-1}\left(\frac{1}{\omega\tau}\right) + \omega\tau\cdot\ln\left(\frac{1+(\omega\tau)^2}{4}\right)\right] \qquad (5.12)$$

The fluctuation relaxation time τ is the same in two dimensions, given in Eq. 5.8.

5.2.2 *Scaling Theories*

The above treatment of the fluctuation conductivity is valid as long as the order parameter is small enough so that the non-linear terms in the expansion of the Ginzburg-Landau free energy can be safely neglected. Under circumstances where the non-linear terms are important, such an expansion of the free energy is no longer valid and other approaches must be adopted. In this section a more general scaling theory will be described, which utilizes dimensional arguments to obtain a form for the conductivity that is valid even when the fluctuations are large.

The general scaling theory for the conductivity[30,49] starts with the assumption that the correlation length ξ diverges as $T \to T_c$ ($\varepsilon \to 0$) as

$$\xi(T) = \frac{\xi_0}{\varepsilon^{\nu}} \qquad (5.13)$$

where the exponent ν can take on any value, and is not restricted to be $\nu=1/2$ as in the Gaussian theory (see Eq. 5.1). To describe the behavior of the conductivity, the theory also assumes a fluctuation relaxation time τ that diverges as $\varepsilon\to 0$ as $\tau \sim \xi^z$, where z is the dynamical critical exponent. Utilizing the temperature dependence of ξ in Eq. 5.13 gives the temperature dependence of τ as

$$\tau(T) = \frac{\tau_0}{\varepsilon^{\nu z}} \qquad (5.14)$$

Once again, z can take on any arbitrary value and is not limited to the Gaussian value of $z=2$ (which gives $\tau \sim 1/\varepsilon$, see Eq. 5.3).

The form of the fluctuation conductivity at finite frequencies can be determined by dimensional arguments and the requirement that the conductivity remain finite as $T\to T_c$. This requires that near T_c the finite frequency conductivity scale with the

correlation length as

$$\sigma(T,\omega) \approx \xi^{2-D+z}\, S_{\pm}(\omega\tau) \tag{5.15}$$

where D is the dimensionality, z is the dynamical critical exponent, and $S_{\pm}(x)$ are temperature-independent scaling functions above (+) and below (-) T_c. The quantity τ is the fluctuation relaxation time defined above (Eq. 5.14). If we write the conductivity as $\sigma=|\sigma|\exp(i\phi_\sigma)$ then the phase of the conductivity should also scale near the phase transition as

$$\phi_\sigma(T,\omega) = \Phi_{\pm}(\omega\tau) \tag{5.16}$$

where once again $\Phi_{\pm}(x)$ are temperature-independent scaling functions.

The scaling functions $S_{\pm}$ and $\Phi_{\pm}$ take on simple limiting forms when $T=T_c$. Given the fact that relaxation time diverges as $\tau \approx \xi^z$, in order that the conductivity remain finite as the ξ diverges, the magnitude of the conductivity must scale with frequency at T_c as

$$|\sigma(T=T_c)| = d|\omega|^{-(2-D+z)/z} \tag{5.17}$$

At $T=T_c$ the phase of the conductivity is a constant independent of frequency that depends only on the dimensionality of the system D and the dynamical critical exponent z:

$$\phi_\sigma(T=T_c) = \frac{\pi}{2}\left[\frac{2-D+z}{z}\right] \tag{5.18}$$

5.3 NORMAL STATE BEHAVIOR: TEMPERATURE DEPENDENCE OF THE DC RESISTIVITY

In order to look for fluctuation effects in our YBCO films, we first examine the temperature dependence of the dc resistivity, which is measured in a separate experiment over the entire temperature range from room temperature down to T_c, and is shown for sample #NCL705b in Fig. 5.1. The dc resistivity is measured after the gold Corbino contacts are evaporated onto the film, in a three-point configuration, with two contacts on the outer circular contact and one on the inner conductor contact pad. Figure 5.2 shows the numerical derivative dρ/dT versus temperature of the same experimental data. Note from the dρ/dT plot that the slope is approximately constant for most of the temperature range from room temperature down to within about 10-20K of T_c, at which point the slope begins to increase, indicative of enhanced conductivity as T_c is approached.

The dc resistivity vs. temperature data is relevant to the high frequency measurements presented here for two reasons. First, the behavior of the temperature dependent dc resistivity can be compared directly with the results of other dc resistivity experiments that show evidence of fluctuation effects. Perhaps more importantly for the finite frequency experiments presented later in this section is the fact that an accurate value for the mean-field (or normal state) resistivity can be extracted from these dc measurements. This can be accomplished because the total conductivity can be assumed to be composed of the sum of a mean-field contribution and a fluctuation contribution:

$\sigma^{tot}(T,\omega) = \sigma^{mf}(T) + \sigma^{fl}(T,\omega)$, where the mean-field term corresponds to a resistivity that is linear in temperature and frequency independent: $\sigma^{mf}(T) = 1/(\rho_0+\rho_1 \cdot T)$. Then by fitting the temperature dependence of the dc resistivity (shown in Fig. 5.1, for example), with an appropriate model for $\sigma^{fl}(T,\omega=0)$, the function $\sigma^{mf}(T)$ can be determined. This mean field contribution is then subtracted from the total conductivity measured at finite frequency to obtain the finite frequency fluctuation conductivity.

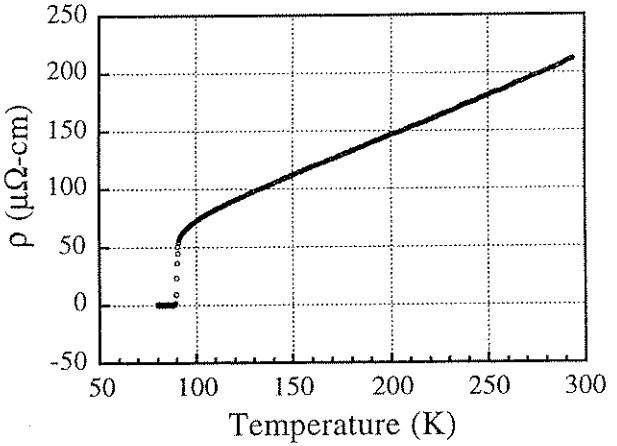

Fig. 5.1. The temperature dependence of the dc resistivity for sample NCL705b.

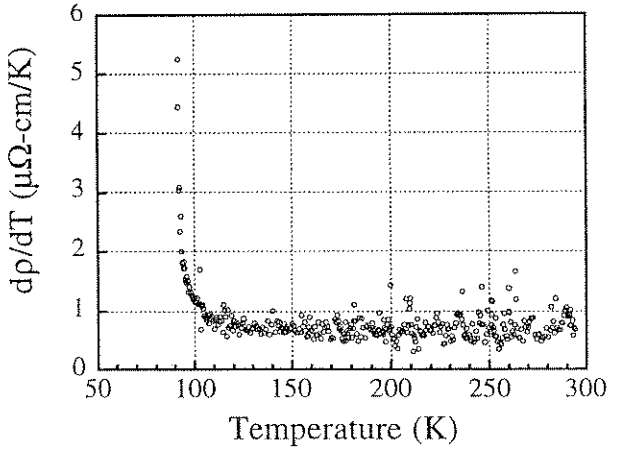

Fig. 5.2. The numerical derivative dρ/dT for the resistivity data in figure 5.1.

The temperature dependence of the dc fluctuation contribution to the conductivity depends on the dimensionality of the system, and is given for three dimensions by Eq. 5.5 and for two dimensions by Eq. 5.10. Because of the layered nature and strong anisotropy of the high T_c superconductors, it is not clear if one

should use the three dimensional isotropic form for the fluctuation conductivity, or the two dimensional form with the film thickness given by the copper-oxide layer separation. In order to take into account the anisotropic nature of the cuprates, Lawrence and Doniach[51] created a model for the fluctuation conductivity which essentially interpolates between the 2D and the 3D forms above, and is given by

$$\sigma'_{LD} = \frac{e^2}{16\hbar d\,\varepsilon}\frac{1}{\left[1+\frac{1}{\varepsilon}\left(\frac{2\xi_c(0)}{d}\right)^2\right]^{1/2}} \qquad (5.19)$$

where here $\xi_c(0)$ is the c-axis correlation length at zero temperature, and d is the inter-layer separation. As can be seen from Eq. 5.19, when the c-axis correlation length is much less than the inter-layer spacing ($\xi_c(0) << d$), the fluctuation conductivity reduces to the 2D Gaussian expression (Eq. 5.10), while in the opposite limit, when $\xi_c(0) >> d$, Eq. 5.26 reduces to the 3-dimensional form (Eq. 5.5).

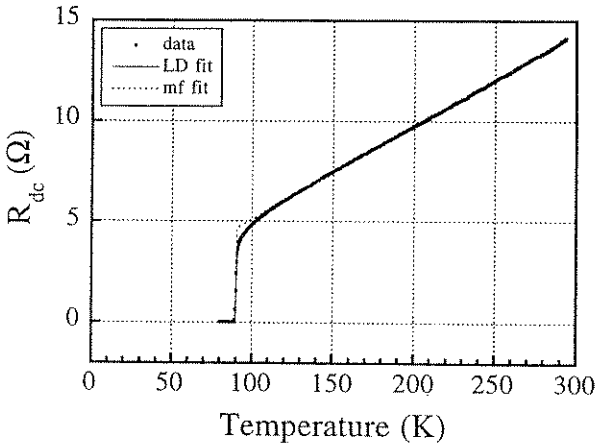

Fig. 5.3. Fits to the dc sheet resistance vs. temperature using both the Lawrence-Doniach model of the fluctuation conductivity (solid line), and using just the mean-field conductivity (dashed line).

With the above forms (2D, 3D, Lawrence-Doniach) for the temperature dependence of $\sigma'^{fl}(T,\omega=0)$, the measured dc resistance can be fit to the 2D and 3D Gaussian fluctuation models, as well as to the Lawrence-Doniach model. For the pure Gaussian models, 4 variable parameters are used: ρ_0, ρ_1, T_c, and either d or ξ_0 (depending on the dimensionality), while for the Lawrence-Doniach model 5 parameters are used: ρ_0, ρ_1, T_c, d, and $\xi_c(0)$. We also attempt to fit the data without any fluctuation effects ($\sigma'^{fl}=0$), using only 3 parameters: ρ_0, ρ_1, and T_c. The results of these fits are given for sample NCL705b in table 5.1. As might be expected, the Lawrence-Doniach model fits the data the best, and this fit is shown along with the data, and also the fit using only the mean-field contribution ($\sigma'^{fl}=0$), in Figs. 5.3 and 5.4. The parameters extracted from the Lawrence-Doniach fit seem to be physically reasonable, with an inter-layer separation of d=10.0 Å, and a c-axis coherence length of $\xi_0 = 0.91$ Å. These parameters give 2D fluctuations in the region far above T_c, which

cross over to 3D fluctuations near T_c. The cross-over from 2D to 3D fluctuations occurs when the temperature-dependent correlation length becomes comparable to half the inter-layer spacing ($\xi_c(0)/\sqrt{\varepsilon} \approx d/2$), which occurs at T = 90.58 K for these fit parameters. These parameters seem to be in reasonable agreement with previous temperature-dependent measurements of the dc conductivity of YBCO crystals[34-36]. In addition, the values for ρ_0 and ρ_1 for the 2D Gaussian, 3D Gaussian, and mean-field fits give values for the mean field resistivity at temperatures near T_c that differ from the Lawrence-Doniach value by at most 5%.

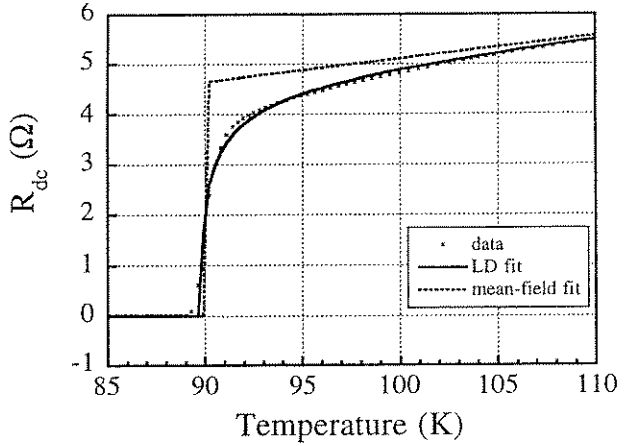

Fig. 5.4. The Lawrence-Doniach (solid line) and mean-field only (dashed line) fits to the dc sheet resistance near T_c.

Table 5.1. Parameters for fits to the dc resistance vs. temperature data for sample #NCL705b. The fit quality is in Ω/degree of freedom, and is a minimum for the best fit.

fit	r_0(μΩ-cm)	r_1(μΩ-cm)	T_c(K)	ξ_0(Å)	d(Å)	fit qual. (χ^2)
mf	7.159	0.694	90.00	–	–	0.076
2D	9.649	0.699	89.52	–	13.0	0.024
3D	4.726	0.793	89.87	1.23	–	0.034
LD	10.490	0.700	89.83	0.91	10.0	0.023

5.4 THE COMPLEX RESISTIVITY NEAR T_c IN YBCO FILMS

The main advantage of the Corbino reflection technique is the ability to measure the complex resistivity $\rho^* = \rho_1 + i\rho_2$ over a wide range of frequencies in the microwave range. Figure 5.5 shows the temperature dependence of ρ_1 at a number of different measurement frequencies for a typical YBCO thin film. Also shown in Fig. 5.5 is the dc resistivity measured as described above in section 5.3. The main feature of the temperature dependent data is the fact that the transition appears to broaden considerable as the measurement frequency increases. In the normal state, the data at different

frequencies (including dc) all describe the same curve, because the normal state scattering rate ($1/\tau_n$) is much greater than the measurement frequency over the entire measurement range

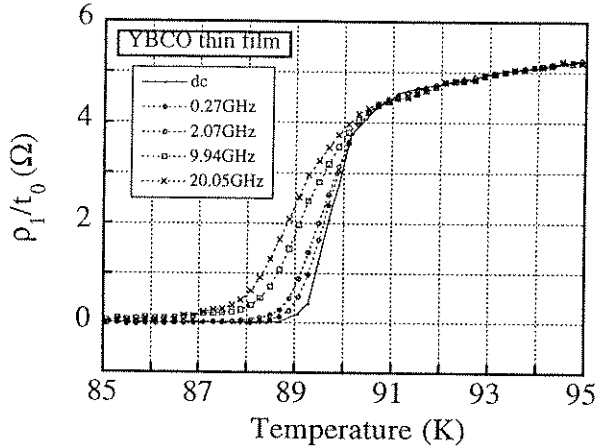

Fig. 5.5. The temperature dependence of ρ_1/t_0 at several different frequencies near the superconducting phase transition.

The temperature dependence of ρ_2/t_0 is shown in Fig. 5.6 at the same measurement frequencies as Fig. 5.5. In the region below T_c, ρ_2/t_0 increases as the measurement frequency increases, and the temperature at which the peak in ρ_2/t_0 occurs moves systematically lower for higher frequencies. Also of note is the fact that $\rho_2/t_0 \approx 0$ for all frequencies in the normal state, consistent with a normal state resistivity that is completely real.

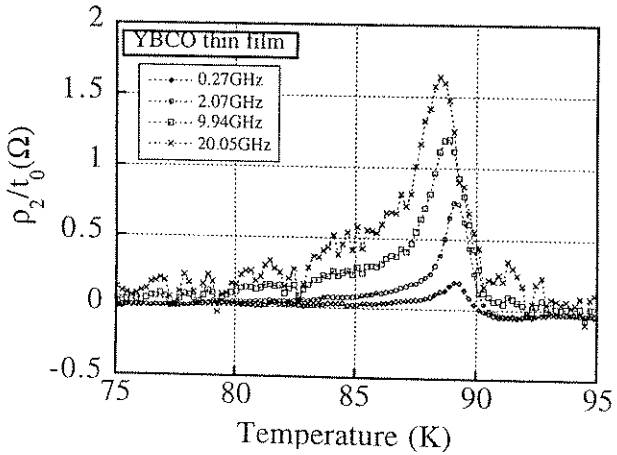

Fig. 5.6. The temperature dependence of ρ_2/t_0 at several different frequencies.

Because the Corbino reflection technique is a swept-frequency measurement, it is possible to directly measure the frequency dependence that is apparent in Figs. 5.5 and 5.6. Figures 5.7 and 5.8 display the frequency dependence of the same sample at several different temperatures in the transition region. Above T_c ρ_1/t_0 is roughly frequency independent, and ρ_2/t_0 is roughly zero, as pointed out in the temperature dependence above. In the midst of transition region both ρ_1/t_0 and ρ_2/t_0 show considerable frequency dependence. At temperatures well below T_c the quantity ρ_1/t_0 is small, and ρ_2/t_0 is approximately linear in frequency, since $\rho_2/t_0 \approx \mu_0\omega\lambda^2(T)/t_0$ for $T<T_c$.

5.5 FLUCTUATION EFFECTS IN THE FREQUENCY DEPENDENT CONDUCTIVITY

In order to analyze the frequency dependent data, it is convenient to convert the measured complex resistivity to a conductivity. It is then simple to remove the mean-field contribution as determined from the dc resistivity fits in order to investigate the frequency dependence of the fluctuation conductivity alone.

5.5.1 *Frequency Dependence at $T=T_c$*

The frequency dependence of the fluctuation conductivity magnitude ($|\sigma|=[\sigma_1^2 + \sigma_2^2]^{1/2}$) and phase ($\phi_\sigma=\tan^{-1}[\sigma_2/\sigma_1]$) in the vicinity of the superconducting phase transition are quantities of considerable interest. According to general scaling theory discussed above,[30,49] the phase angle of the fluctuation conductivity should take on a frequency-independent value at the critical temperature T_c that depends only on the dimensionality D of the system and the dynamical critical exponent z (see Eq. 5.18): $\phi_\sigma(T=T_c) = (\pi/2)\cdot(2\text{-}D+z)/z$. The corresponding behavior of the magnitude of the fluctuation conductivity is a power-law frequency dependence at $T=T_c$ (see Eq. 5.17): $|\sigma^{fl}(T=T_c)| \sim |\omega|^a$, with $a=(2\text{-}D+z)/z$. The frequency dependence of the magnitude and phase of the fluctuation conductivity can therefore be examined to locate the critical temperature, and to obtain a value for the dynamical critical exponent z assuming D is known.

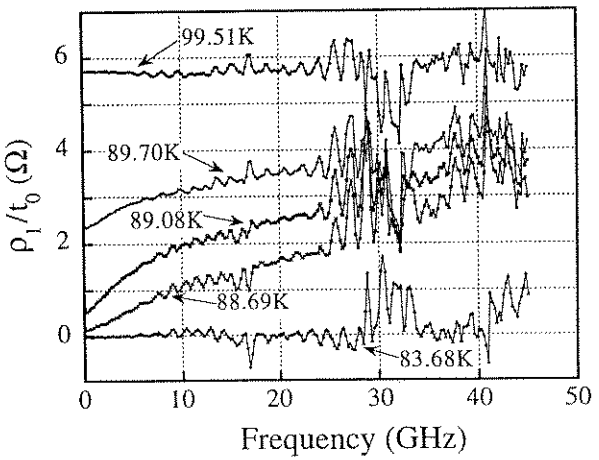

Fig. 5.7. The frequency dependence of ρ_1/t_0 at temperatures in the vicinity of T_c.

The measured frequency dependence of the magnitude and phase of the fluctuation conductivity is shown in Figs. 5.9 and 5.10 respectively at temperatures in the vicinity of T_c. The fluctuation conductivity is extracted from the total measured conductivity by subtracting off the frequency-independent value for the mean-field conductivity. It should be noted that using a different value for $\sigma^{mf}(T)$ within the range given in table 5.1 (roughly ±5%) does not affect the results. To determine the critical isotherm we fit the frequency dependence of the magnitude of the fluctuation conductivity in Fig. 5.9 to a power law as prescribed by Eq. 5.17, and obtain the best fit for the data at T=89.18 K, where $|\sigma(\omega)| \sim \omega^{-0.62\pm0.02}$. Examination of Fig. 5.10 shows that the fluctuation conductivity phase angle takes on a roughly constant value also for the T=89.18 K data set, with a mean value of $\phi_\sigma=0.64\cdot(\pi/2)$ and a standard deviation of $0.12\cdot(\pi/2)$. Note that for temperatures above (below) 89.18 K, the phase is an increasing (decreasing) function of frequency. The frequency dependence at T = 89.18 K shows that the value of the power law of the fluctuation conductivity magnitude and the value of the (constant) reduced phase angle are the same (within experimental error), in agreement with the prediction of the scaling theory (Eqs. 5.17 and 5.18).

The values of the phase angle and the magnitude power law determine the value of the dynamical critical exponent z. However, since the data sets are taken at 0.2 K intervals, there exists some uncertainty in the exact determination of T_c from the frequency dependence of the conductivity. This uncertainty is estimated to be roughly half the separation in temperature between the data sets, which is 0.1 K. Due to this uncertainty in T_c there also exists a corresponding uncertainty in the determination of the critical phase angle and power law values. We can therefore conclude from the behavior of the frequency dependent fluctuation conductivity that the thermodynamic critical temperature for this sample is T_c = 89.18 ± 0.1 K and the value of the dynamical critical exponent (with the assumption that D=3) is in the range z = 2.35-2.95. Other samples give values for z as high as z=3. In all cases our results for the value of the dynamical critical exponent are significantly larger than the Gaussian prediction of z=2. Since the fluctuation relaxation time τ^{fl} diverges as $\tau \sim \xi^z$, the fact that z > 2 suggests critical behavior in our samples. Other experimental determinations of the dynamical critical exponent z from non-linear dc resistivity measurements give widely varying results, from z=2.2±0.4[52] up to z=8.3±0.3.[53]

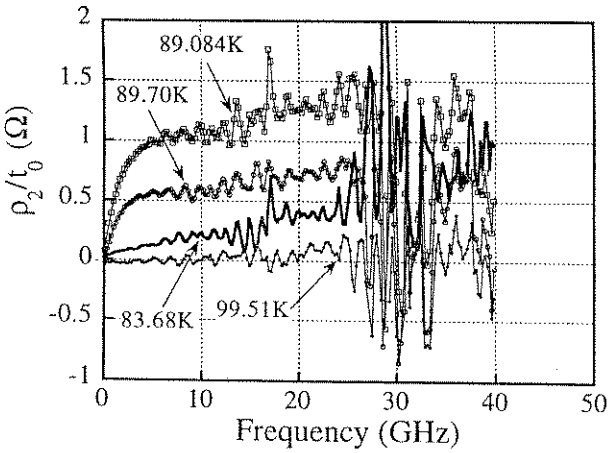

Fig. 5.8. The frequency dependence of ρ_2/t_0 at temperatures in the vicinity of T_c.

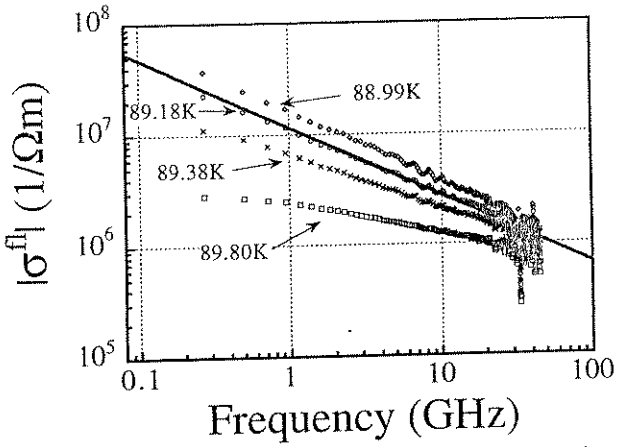

Fig. 5.9. Magnitude of the fluctuation conductivity in the vicinity of T_c. The solid line is a power law fit to the T=89.18K with a power of -0.62.

5.5.2 *Scaling of the Frequency-dependent Conductivity above T_c*

The results obtained in section 5.5.1 for the dynamical critical exponent at T_c suggest that we look for scaling behavior in the frequency-dependent fluctuation conductivity at temperatures above T_c. From scaling theory it is expected that in the vicinity of a phase transition, the fluctuation conductivity should scale with the appropriate power of the (temperature-dependent) correlation length ξ and the fluctuation lifetime τ^{fl}, as shown in Eq. 5.15. The function S_+ (S_-) in Eq. 5.15 is the universal scaling function above

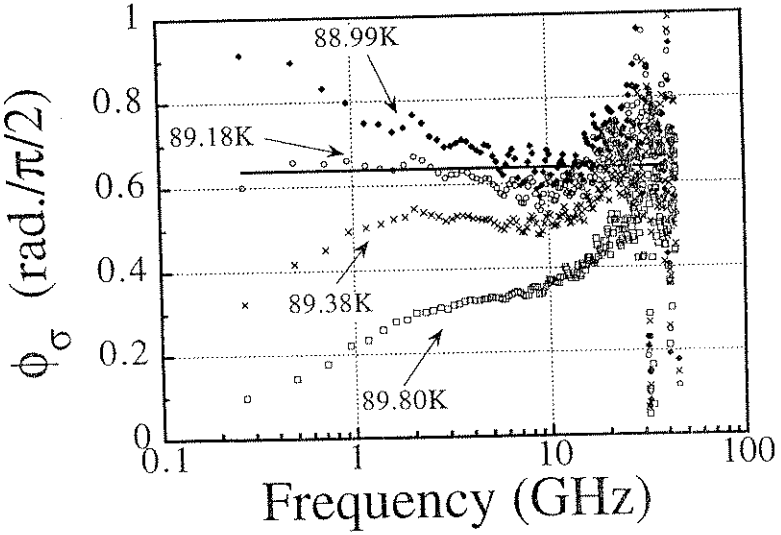

Fig. 5.10. Reduced phase of the fluctuation conductivity in the vicinity of T_c. The solid line is a constant value of 0.64.

(below) T_c, which should be the same for all members of a given universality class, as should be the critical exponents ν and z. With the assumption that D=3, Eq. 5.15 implies that the quantity $\sigma/\varepsilon^{-\nu(z-1)}$ plotted vs. the scaled frequency $\omega\,\varepsilon^{-\nu z}$ should yield the universal scaling function S_+. We can determine if our measured data obeys Eq. 5.22 by plotting the scaled conductivities, measured at different temperatures, vs. the scaled frequency and varying the parameters ν, z, and T_c until the different data sets all collapse onto the same universal curve. We have determined already from the behavior of the critical isotherm (section 5.5.1) that $T_c = 89.18 \pm 0.1$ K and $z \approx 2.6$, leaving just the value of ν which can be adjusted to collapse the data.

Figure 5.11 shows conductivity data from 5 different temperatures which collapses onto a single curve when scaled as described above with T_c = 89.10 K, z=2.6, and ν=1.2. In the inset to Fig. 5.11 we have plotted the magnitude of the scaling function for D=3 in the Gaussian theory, which was first derived by Schmidt.[48] The two functions are qualitatively similar, however the scaling function that describes the data approaches a power law of -0.62 at large argument, while the 3D Gaussian scaling function approaches a power law of -0.50. The scaling behavior is relatively insensitive to the ultimate choice of T_c (within the above quoted error), although the value of ν varies in the range ($1.0 < \nu < 1.2$) as a result of the specific choice of T_c. If the value of ν is fixed at $\nu = 2/3$ (which is the prediction of the 3D XY model), then the data does show scaling behavior if the value of z is increased to approximately z= 3.5. Such a large value of z is inconsistent, however, with the conclusions of section 5.5.1.

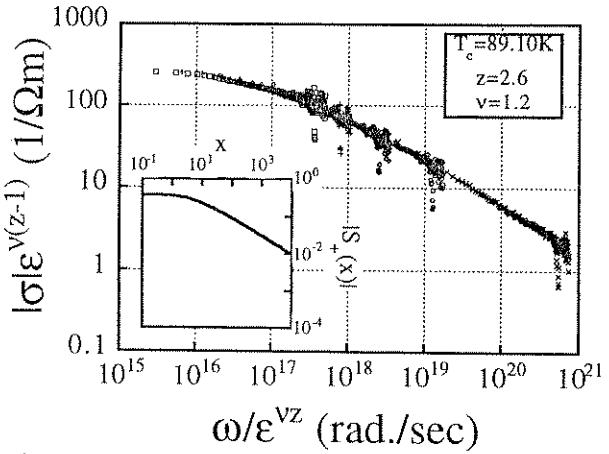

Fig. 5.11. Scaling behavior of the magnitude of the fluctuation conductivity. The data sets shown are 89.18 K (x's), 89.38K (circles), 89.58K (diamonds), 89.80K (+'s), and 90.00K (squares).

While the magnitude of the fluctuation conductivity obeys the scaling relation given by Eq. 5.15, the phase of the fluctuation conductivity scales with the relation given by Eq. 5.16. When we plot our (unscaled) measured conductivity phase angles vs. the scaled frequency, **with the same values for ν, z, and T_c that we used to scale the magnitude of the conductivity**, we obtain the results shown in Fig. 5.12. Although the phase data shows more uncertainty than the magnitude data, it confirms the scaling behavior seen in the conductivity magnitude data. We have also plotted the 3D Gaussian scaling function for the conductivity phase angle in the inset to

Fig. 5.12, which shows a similar functional dependence to our data, but reaches a maximum value of 0.5 for large argument, whereas the function that describes our data approaches roughly 0.64.

We conclude from the frequency dependent data that both the magnitude and phase of our measured fluctuation conductivities show scaling behavior with ~ 1 K of T_c with the same values for the critical exponents $\nu \approx 1.0$-1.2 and $z \approx 2.35$-2.95. In spite of the uncertainty in the exact values of the critical exponents ν and z, these results mean physically that the fluctuation lifetime diverges as $T \rightarrow T_c$ from above roughly as $\tau^{fl} \sim 1/\varepsilon^{\nu z} \approx 1/\varepsilon^3$, which is significantly faster than the Gaussian prediction of $\tau^{fl} \sim 1/\varepsilon$. Our measurements therefore represent a direct observation of the slowing down of the fluctuation relaxation rate $1/\tau^{fl}$ as $T \rightarrow T_c$ from above.

5.6. TEMPERATURE DEPENDENCE OF THE FLUCTUATION CONDUCTIVITY

In order to view our fluctuation conductivity data from a different perspective, we plot in figure 5.13 the temperature dependence of the fluctuation conductivity at several fixed frequencies. The value of T_c used to calculate ε is T_c=89.10 K, as determined from the scaling above, and the mean field contribution $\sigma^{mf}(T)$ has been subtracted off. This figure illustrates the effect of the fluctuation relaxation rate $1/\tau^{fl}$ passing through the measurement frequencies. At dc, the fluctuation conductivity diverges as $\varepsilon \rightarrow 0$. At finite frequency the existence of a finite fluctuation lifetime means that the fluctuation conductivity divergence will be cut off when $\omega \sim 1/\tau^{fl}$. The points indicated by arrows indicate the estimated temperature at which $\omega\tau^{fl} \sim 1$ for measurement frequencies of 10 GHz, 2 GHz, and 0.5 GHz. If the conductivity obeyed the Gaussian theory, all the curves would remain together until $\varepsilon \sim 1 \times 10^{-3}$ for the measurement frequencies in Fig. 5.13. In the inset to Fig. 5.13 we plot the ε dependence of τ^{fl} derived as described above, along with the strict Gaussian calculation of τ^{fl} ($\sim 1/\varepsilon$), Eq. 5.8. The dashed line is a power law fit to $\tau^{fl} \sim 1/\varepsilon^3$, which is consistent with the ε dependence of τ^{fl} determined from the frequency dependence ($\tau^{fl} \sim 1/\varepsilon^{\nu z} \approx 1/\varepsilon^{3.1}$), within experimental error. Figure 5.13 represents further evidence that the fluctuation lifetime diverges much faster than the Gaussian prediction as $\varepsilon \rightarrow 0$.

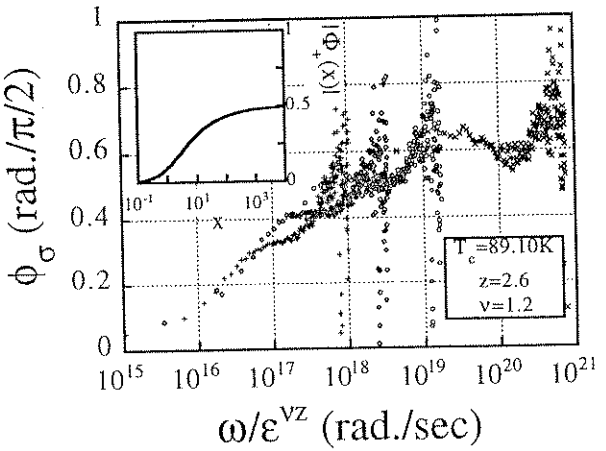

Fig. 5.12. Scaling of the fluctuation conductivity phase. The data sets shown are 89.18 K (x's), 89.38K (circles), 89.58K (diamonds), and 89.80K (+'s).

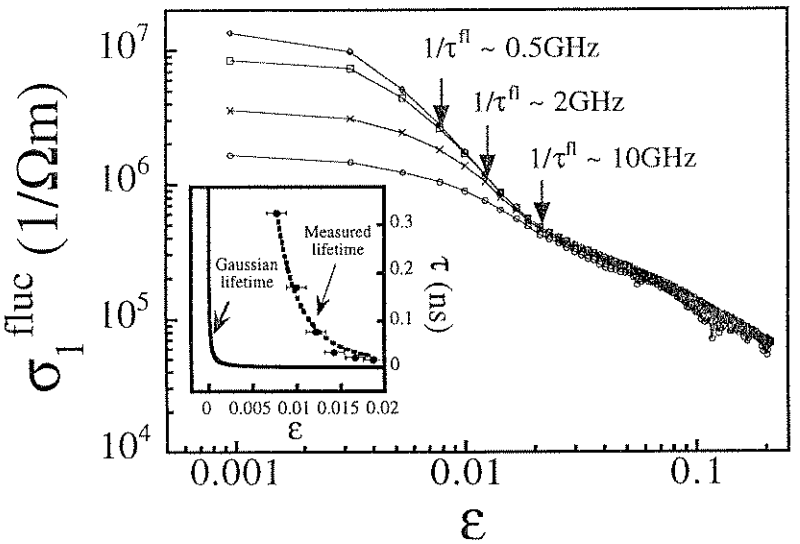

Fig. 5.13 The fluctuation conductivity σ_1 vs. $\varepsilon=\ln(T/T_c)$, at 10 GHz (circles), 2 GHz (x's), 0.5 GHz (squares), and 0.27 GHz (diamonds). The arrows indicate approximately where $1/\tau^{fl}$ is equal to the measurement frequency. The inset shows the temperature dependence of τ^{fl} derived in this manner, along with the temperature dependence of τ^{fl} in the Gaussian theory.

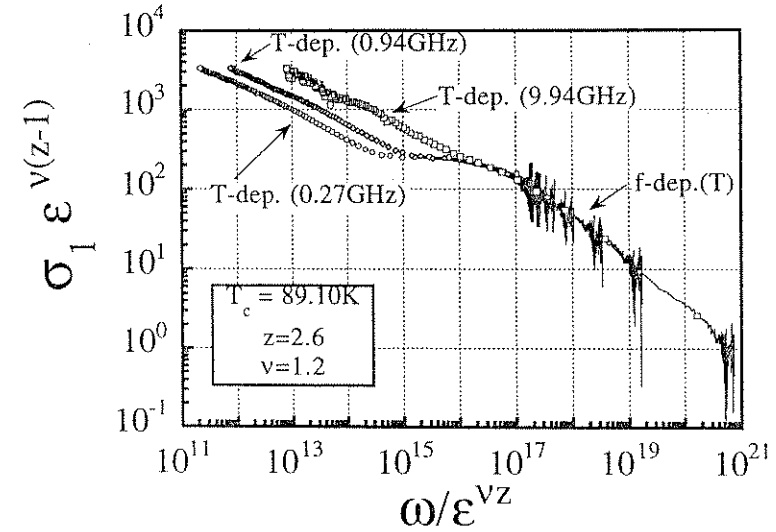

Fig. 5.14. The scaled temperature dependence of σ_1 at fixed frequency (symbols), along with the scaled frequency dependence at six different fixed temperatures (solid lines), all with T_c=89.10K, ν=1.2, and z=2.6.

Using the critical exponents for this sample determined from the frequency dependence analysis, we should also be able to scale the temperature dependence of σ_1 in Fig. 5.13 according to the scaling relation in Eq. 5.15, so that the data within the scaling region will collapse together. This is just what we observe in Fig. 5.14, where the scaled temperature dependence measured at three discrete frequencies is plotted along with the scaled frequency dependence of σ_1 measured at 6 different temperatures, all with the same values of T_c, ν, and z. This figure shows dramatically how both the temperature dependence and the frequency dependence of the fluctuation conductivity are both described by the single universal scaling function S_+ within the scaling regime. The point at which the temperature-dependent data deviate from the universal curve indicate the temperature at which the sample leaves the scaling regime (T ~ T_c+ 2 K).

5.7. SAMPLE DEPENDENCE OF FLUCTUATION EFFECTS

Before concluding it is necessary to address the question of what effect the presence of material disorder and inhomogeneity have on the above results. We address this question experimentally by measuring samples with varying amounts of disorder, as measured by high resolution x-ray diffraction.[54] (The x-ray measurements are performed by S. B. Qadri and E. F. Skelton of the Naval Research Laboratories.) If our samples all belong to the same universality class then we expect them all to follow the same universal function with the same critical exponents as described above. In Fig. 5.15 we plot the scaled temperature dependence (with ν=1.2 and z=2.6) of the fluctuation conductivity for thin film #NCL705b, along with the scaled temperature dependence of a second thin film (thin film #RAY7) and also a single crystal, all measured at approximately 10 GHz. The conductivity of the single crystal was measured using a cavity perturbation method.[37] Sample RAY7 has a broader resistivity transition width than film NCL705b, and the high resolution x ray diffraction results show that film RAY7 has a larger distribution of oxygen content, from which we conclude that film RAY7 is the more disordered of the two films.

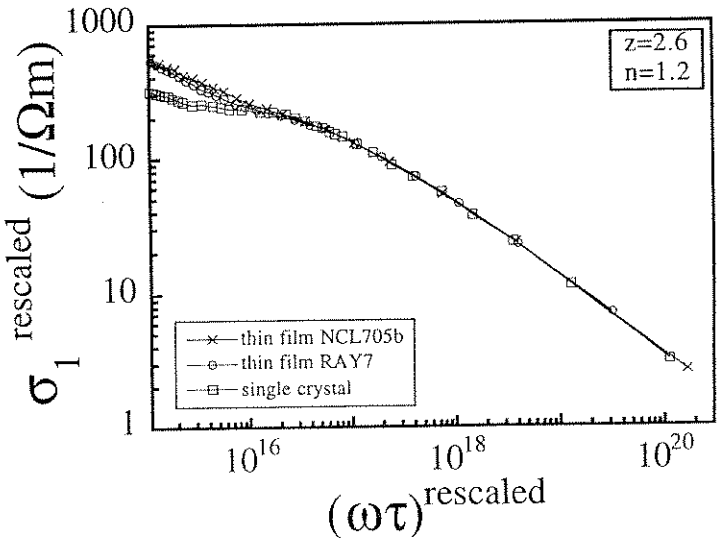

Fig. 5.15. The scaling of the temperature dependence of the fluctuation conductivity measured at approx. 10 GHz for 2 different thin film samples and a single crystal sample.

In order to have the data from these 3 very different samples collapse onto the same curve, it is necessary only to adjust the non-universal values of τ_0 and ξ_0 in the quantities $\xi = \xi_0/\varepsilon^{\nu}$ and $\tau = \tau_0/\varepsilon^{\nu z}$ in Eqs. 5.13 and 5.14. The relative values for τ_0 and ξ_0 used to scale the data in Fig. 5.15 are given in table 5.2. If the single crystal is assumed to represent the least disordered sample, than table 5.2 indicates that the "bare" relaxation time τ_0 decreases with increasing disorder. Fig. 5.15 illustrates that our scaling results are relatively insensitive to disorder. This might be expected from the Harris criterion,[55] which predicts that if the specific heat exponent α is negative (which appears to be the case for YBCO[39]), then disorder should not affect the universality of the critical exponents and scaling functions.

Table 5.2. Relative values of the non-universal parameters τ_0 and ξ_0 for the different samples shown in Fig. 5.15.

Sample	$\xi_0/(\xi_0^{\text{film\#NCL705b}})$	$\tau_0/(\tau_0^{\text{film\#NCL705b}})$
thin film # NCL705b	1	1
thin film #RAY7	0.625	0.5
single crystal	1	11

6. Conclusions

We have measured the fluctuation conductivity over three orders of magnitude in frequency in the vicinity of T_c for YBCO thin films. From the frequency dependence of $\sigma^{fl}(T, \omega)$ we have determined the thermodynamic critical temperature and the dynamical critical exponent $z = 2.35$ to 3.0, extracted the fluctuation lifetime as a function of temperature, and shown that the divergence of the fluctuation lifetime is much faster than what the Gaussian theory predicts (all corroborated by scaling analysis), consistent with critical slowing down of the fluctuation relaxation rate for $T - T_c < 1$ to 2 K in YBCO thin films. Further results and discussion are given in reference [56].

7. References

1. A.B. Pippard, Proc. Roy. Soc. **A191**, 370 (1947).
2. R.E. Glover, III, and M. Tinkham, Phys. Rev. **108**, 243 (1957).
3. J.G. Bednorz and K.A. Müller, Z. fur Phys **64**, 189 (1986).
4. M.K. Wu, J.R. Ashburn, C.J. Torng, P.H. Hor, R.L. Meng, L. Gao, Z.J. Huang, Y. Q. Wang, C.W. Chu, Phys. Rev. Lett. **58**, 908 (1987).
5. W. N. Hardy et al., Phys. Rev. Lett. **70**, 3999 (1993).
6. Jian Mao, D. H. Wu, J.L. Peng, R.L. Greene, and Steven M. Anlage, Phys. Rev. B **51**, 3316 (1995).
7. Jian Mao, Ph. D. thesis, University of Maryland, 1995.
8. Dong-Ho Wu and S. Sridhar, Phys. Rev. Lett., **65**, 2074 (1990).
9. J.C. Booth, Dong Ho Wu, and Steven M. Anlage, Rev. Sci. Instrum. **65**, 2082 (1994).
10. H.K. Olsson, R.H. Koch, W. Eidelloth, and R.P. Robertazzi, Phys. Rev. Lett. **66**, 2661 (1991).
11. N.-C. Yeh, D.S.Reed, W. Jiang, U. Kriplani, F. Holtzberg, A. Gupta, B.D. Hunt, R.P. Vasquez, M.C. Foote, and L. Bajuk, Phys. Rev. B **45**, 5654 (1992).

12. H. Wu, N.P. Ong, and Y.Q. Li, Phys. Rev. Lett. **71**, 2642 (1993).
13. S. Ramo, J.R. Whinnery, and T. Van Duzer, "Fields and Waves in Communication Electronics", Second Edition, John Wiley and Sons, New York (1984), p.225.
14. O.M. Corbino, Nuovo Cimento **1** (1911); R.P. Heubener, "Magnetic Flux Structures in Superconductors" (Springer, Berlin, 1979), p.128.
15. M.P. Shaw and P.R. Solomon, Phys. Rev. **164**, 535 (1967).
16. N. Bluzer, D.K. Fork, T.H. Geballe, M.R. Beasley, M.Y. Reizer, S.R. Greenfield, J.J. Stankus, and M. Fayer, IEEE Trans. Magn. 27, 1519 (1991); N. Bluzer, J. Appl. Phys. **71**, 1336 (1992).
17. Yan-Zhen Wei and S. Sridhar, Rev. Sci. Instrum. **60**, 3041 (1989).
18. L. L. Li, N. H. Ismail, L. S. Taylor, and C. C. Davis, IEEE Trans. Biomed. Eng. **39**, 49 (1992).
19. Nour-Eddine Belhadj-Tahar, A. Fourrier-Lamar, and H. DeChanterac, IEEE Trans. Microwave Theory Tech. **38**, 1 (1990).
20. M. A. Saed, S. M. Riad, and W. A. Davis, IEEE Trans. Microwave Theory Tech. **39**, 485 (1990).
21. This coaxial cable is manufactured by Rogers Corporation.
22. The microwave connector used is a V101-F connector, made by Wiltron Corp.
23. D.T. Dijikkamp, T. Venkatesan, X.D. Wu, S.A. Shaheen, N. Jisrawi, Y.H. Min-Lee, W.L. McLean, and M. Croft, Appl. Phys. Lett. **51**, 619 (1987).
24. J.C. Booth, Ph.D. Thesis, University of Maryland (1996).
25. D. Misra, M. Chabbra, B.R. Epstein, M. Mirotznik, and K.R. Foster, IEEE Trans. Microwave Theory Tech. **38**, 8 (1990).
26. M.A. Stuchly and S.S. Stuchly, IEEE Trans. Instrum. Meas. **29**, 176 (1980).
27. E.C. Burdette, F.L. Cain, and J. Seals, IEEE Trans. Microwave Theory Tech. **28**, 414 (1980).
28. G.B. Gajda and S.S. Stuchly, IEEE Trans. Microwave Theory Tech. **31**, 380 (1983).
29. M. Razaz and J.B. Davies, IEEE Trans. Microwave Theory Tech. **27**, 564 (1979).
30. D. S. Fisher, M. P. A. Fisher, and D. Huse, Phys. Rev B **43**, 130 (1991).
31. C. J. Lobb, Phys. Rev. B **36**, 3930 (1987).
32. S. L. Lehoczky, and C. V. Briscoe, Phys. Rev. Lett. **24**, 880 (1970); S. L. Lehoczky, and C. V. Briscoe, Phys. Rev B **4**, 3938 (1971).
33. D. B. Tanner, Phys. Rev B **8**, 5045 (1973).
34. M. B. Salamon in "Physical Properties of High Temperature Superconductors I", D. Ginsberg, Ed., World Scientific, Singapore (1989).
35. S. J. Hagen, Z. Z. Wang, and N. P. Ong, Phys. Rev B **38**, 7137 (1988).
36. T. A. Friedmann, J. P. Rice, J. Giapintzakis, and D. M. Ginsberg, Phys. Rev B **39**, 4258 (1989).
37. Steven M. Anlage, J. Mao, J. C. Booth, Dong Ho Wu, and J. L. Peng, Phys. Rev B **53**, 2792 (1996).
38. S. Kamal, D. A. Bonn, N. Goldenfeld, P. J. Hirschfeld, Ruixing Liang, and W. N. Hardy, Phys. Rev. Lett. **73**, 1845 (1994).
39. N. Overend, M.A. Howson, I.D. Lawrie, Phys. Rev. Lett. **72**, 3238 (1994).
40. H. K. Olsson, R. H. Koch, W. Eidelloth, and R. P. Robertazzi, Phys. Rev. Lett. **66**, 2661 (1991).
41. H. Wu, N. P. Ong, and Y. Q. Li, Phys. Rev. Lett. **71**, 2462 (1993).
42. D.H. Wu *et al.*, Phys. Rev. Lett. **75**, 525 (1995).
43. N.-C. Yeh, D. S. Reed, W. Jiang, U. Kriplani, C. C. Tsuei, C. C. Chi, and F. Holtzberg, Phys. Rev. Lett. **71**, 4043 (1993).
44. T.P. Orlando and K.A. Delin, "Foundations of Applied Superconductivity", Addison-Wesley, Reading, MA (1991).

45. P.G. deGennes, "Superconductivity of Metals and Alloys", Addison-Wesley, Reading, MA (1966).
46. M. Tinkham, "Introduction to Superconductivity", Robert E. Krieger Publishing Company, Malabar, FL (1975).
47. W.J. Skocpol and M. Tinkham, Rep. Prog. Phys. **38**, 1049 (1975).
48. H. Schmidt, Z. Phys. **216**, 336 (1968); H. Schmidt, Z. Phys. **232**, 443 (1970)
49. A. T. Dorsey, Phys. Rev B **43**, 7575 (1991).
50. L. G. Aslamazov and A. I. Larkin , Fiz. Tverd. Tela **10**, 1104 (1968) [Sov. Phys. Solid State **10**, 875 (1968)].
51. W. E. Lawrence and S. Doniach, Proceedings of the Twelfth International Conference on Low-Temperature Physics, Kyoto, 1970, edited by E. Kanda (Keigaku, Tokyo, 1970), p. 361.
52. C. Dekker *et al.*, Physica C **185-189**, 1799 (1991).
53. J.M. Roberts *et al.*, Phys. Rev. B **51**, 15281 (1995).
54. E.F. Skelton *et al.*, SPIE Proceedings **1516**, 160, W. Yun, Ed. (1995).
55. A.B. Harris, J. Phys. C **7**, 1671(1974).
56. J. C. Booth, *et al.*, Phys. Rev. Lett., Nov. 18, 1996.

FLUCTUATION PHENOMENA IN TUNNEL AND JOSEPHSON JUNCTIONS

A.BARONE

Dipartimento di Scienze Fisiche, Universitá di Napoli "Federico II"
and
Istituto Nazionale per la Fisica della Materia
p. Tecchio, 80,
Napoli, Italy

AND

A.A.VARLAMOV

Istituto Nazionale di Fisica della Materia
Laboratorio "Forum"
Dipartimento di Fisica, Universitá di Firenze
L.E.Fermi, 2 Firenze 50125, Italy
and
Moscow Institute of Steel and Alloys
Leninsky prospect 4,
117936 Moscow, Russia

1. Introduction.

The Josephson junction is a unique object whose properties may be strongly affected by fluctuations of diverse origins. Among them let us mention the usual superconducting (order parameter) fluctuations in the electrodes, thermal noise current fluctuations and, finally, purely quantum fluctuations of the relative Josephson phase (microscopic quantum tunneling). The goal of this review is to consider all of them and to discuss their manifestation in measurable characteristics of Josephson junctions, i.e. voltage-current characteristics, critical current and spectral power.

M. Ausloos and A.A. Varlamov (eds.),
Fluctuation Phenomena in High Temperature Superconductors, 179–199.